SINGULAR VALUE DECOMPOSITIONS FOR SINGLE-CURL OPERATORS IN THREE-DIMENSIONAL MAXWELL'S EQUATIONS FOR COMPLEX MEDIA*

RUEY-LIN CHERN†, HAN-EN HSIEH‡, TSUNG-MING HUANG§, WEN-WEI LIN¶, AND WEICHUNG WANG‖

Abstract. This article focuses on solving the generalized eigenvalue problems (GEP) arising in the source-free Maxwell equation with magnetoelectric coupling effects that models three-dimensional complex media. The goal is to compute the smallest positive eigenvalues, and the main challenge is that the coefficient matrix in the discrete Maxwell equation is indefinite and degenerate. To overcome this difficulty, we derive a singular value decomposition (SVD) of the discrete single-curl operator and then explicitly express the basis of the invariant subspace corresponding to the nonzero eigenvalues of the GEP. Consequently, we reduce the GEP to a null space free standard eigenvalue problem (NFSEP) that contains only the nonzero (complex) eigenvalues of the GEP and can be solved by the shift-and-invert Arnoldi method without being disturbed by the null space. Furthermore, the basis of the eigendecomposition is chosen carefully so that we can apply fast Fourier transformation (FFT)-based matrix vector multiplication to solve the embedded linear systems efficiently by an iterative method. For chiral and pseudochiral complex media, which are of great interest in magnetoelectric applications, the NFSEP can be further transformed to a null space free generalized eigenvalue problem whose coefficient matrices are Hermitian and Hermitian positive definite (HHPD-NFGEP). This HHPD-NFGEP can be solved by using the invert Lanczos method without shifting. Furthermore, the embedded linear system can be solved efficiently by using the conjugate gradient method without preconditioning and the FFT-based matrix vector multiplications. Numerical results are presented to demonstrate the efficiency of the proposed methods.

Key words. Singular value decomposition, null space free method, discrete single-curl operator, the Maxwell equations, chiral medium, pseudochiral medium.

AMS subject classifications. 65F15, 65T50, 15A18, 15A23.

1. Introduction.

Understanding the eigenstructure of the discrete single-curl operator $\nabla\times$ is key to developing efficient numerical simulations for complex materials that are modeled by the Maxwell equations. Biisotropic and bianisotropic materials are two important classes of complex materials [31]. They have constantly drawn intensive studies in physical properties and applications. For example, bianisotropic media are a special type of materials whose properties are characterized by the magnetoelectric as well as the permittivity and permeability tensors [18, 26]. Due to the strong modulation of the wave that arises from the magnetoelectric couplings, counterintuitive features such as negative refraction and backward waves may appear in bianisotropic media [1, 5, 22, 29]. From the mathematical point of view, the distinctive feature associated with bianisotropic media is the single-curl operator in addition to the double-curl operator in the wave equation, which essentially changes the characters of the eigenwaves.

*Version January 11, 2015

†Institute of Applied Mechanics, National Taiwan University, Taipei 106, Taiwan (chernrl@ntu.edu.tw)

‡Department of Mathematics, National Taiwan University, Taipei 106, Taiwan (D99221002@ntu.edu.tw).

§Department of Mathematics, National Taiwan Normal University, Taipei 116, Taiwan (min@ntnu.edu.tw).

¶Department of Applied Mathematics, National Chiao Tung University, Hsinchu 300, Taiwan (wwlin@math.nctu.edu.tw).

‖Institute of Applied Mathematical Sciences, National Taiwan University, Taipei 106, Taiwan (wwang@ntu.edu.tw).

Mathematically, the propagation of electromagnetic waves in biisotropic and bianisotropic materials is modeled by the three-dimensional (3D) frequency domain source-free Maxwell equations [31] with a set of constitutive relations. In particular, we have

$$\nabla \times E = \mathrm{i}\omega B, \quad \nabla \cdot B = 0, \tag{1.1a}$$
$$\nabla \times H = -\mathrm{i}\omega D, \quad \nabla \cdot D = 0. \tag{1.1b}$$

where ω represents the frequency and ε represents the permittivity. E and H are the electric and magnetic fields, respectively. Based on the Bloch theorem [17], we aim to find the Bloch eigenfunctions E and H satisfying the quasi-periodic conditions

$$E(\mathbf{x} + \mathbf{a}_\ell) = e^{\mathrm{i}2\pi\mathbf{k}\cdot\mathbf{a}_\ell} E(\mathbf{x}), \quad H(\mathbf{x} + \mathbf{a}_\ell) = e^{\mathrm{i}2\pi\mathbf{k}\cdot\mathbf{a}_\ell} H(\mathbf{x}) \tag{1.2}$$

for $\ell = 1, 2, 3$ [23]. Here, $\mathbf{a}_1$, $\mathbf{a}_2$, and $\mathbf{a}_3$ are the lattice translation vectors. In this paper, we consider the simple cubic lattice vectors $\mathbf{a}_\ell = a\mathbf{e}_\ell$, where $\mathbf{e}_\ell$ is the ℓ-th unit vector in $\mathbb{R}^3$ and a is a lattice constant. Without loss of generality, we set $a = 1$ throughout this paper. Note that all of the techniques developed here can be applied to face-centered cubic lattice media. The Bloch wave vector in the first Brillouin zone is denoted as $2\pi\mathbf{k}$ [15]. B and D satisfy the constitutive relations

$$B = \mu H + \zeta E \text{ and } D = \varepsilon E + \xi H, \tag{1.3}$$

where μ represents the permeability, and ξ and ζ are magnetoelectric parameters [26, p. 26], [31, p. 44]. Note that ε, μ, ξ, and ζ are 3-by-3 matrices in various forms for describing different types of materials.

The Maxwell equations (1.1) can be rewritten as the following quadratic eigenvalue problems (QEP), which are separate wave equations in terms of E and H.

$$\nabla \times \mu^{-1}\nabla \times E - \mathrm{i}\omega \left[\nabla \times \left(\mu^{-1}\zeta E\right) - \xi\mu^{-1}\nabla \times E\right] - \omega^2 \left(\varepsilon - \xi\mu^{-1}\zeta\right) E = 0; \tag{1.4a}$$
$$\nabla \times \varepsilon^{-1}\nabla \times H - \mathrm{i}\omega \left[\zeta\varepsilon^{-1}\nabla \times H - \nabla \times \left(\varepsilon^{-1}\xi H\right)\right] - \omega^2 \left(\mu - \zeta\varepsilon^{-1}\xi\right) H = 0. \tag{1.4b}$$

In the one-dimensional case, we can apply the quasi-periodic conditions (1.2) to (1.4) and then explicitly define the relations between $\mathbf{k}$ and ω [2, 3, 4, 6, 19]. For higher dimensions, however, solving Eq. (1.2) efficiently remains an open question. We illustrate the difficulty by the following example. An explicit eigendecomposition of the discrete double-curl operator $\nabla \times \nabla \times$ is derived in [11]. Applying this eigendecomposition and assuming $\mu = 1$ and $\zeta = \xi = 0$, we can explicitly derive the invariant subspace of all nonzero eigenvalues corresponding to the (discrete) eigenvalue problem (1.4a). Based on the invariant subspace, efficient numerical methods can be developed to solve (1.4a). However, it is not possible to apply this technique to solve the quadratic eigenvalue problems (1.4) with $\zeta \neq 0$ and $\xi \neq 0$ due to the following difficulties. (i) The eigendecomposition of the discrete double-curl operator in [11] cannot be applied to solving the QEP directly because Eq. (1.4) contains both double- and single-curl operators. (ii) In general, the double- and single-curl operators in (1.4) cannot be diagonalized simultaneously. Furthermore, should we find the eigendecomposition of the single-curl operator, this decomposition cannot be applied to solve the QEP directly because the single-curl operator terms in (1.4), e.g., $\nabla \times (\mu^{-1}\zeta E)$ and $\xi\mu^{-1}\nabla \times E$, are coupled with other terms such as $\mu^{-1}\zeta$ and $\xi\mu^{-1}$. (iii) It is difficult to find the invariant subspace corresponding to the nonzero eigenvalues in the quadratic eigenvalue problems.

While solving (1.4) is not recommended, we focus instead on the original Maxwell equations (1.1) and rewrite it as a coupled generalized eigenvalue problem (GEP)

$$\begin{bmatrix} \nabla\times & 0 \\ 0 & \nabla\times \end{bmatrix} \begin{bmatrix} E \\ H \end{bmatrix} = \mathrm{i}\omega \begin{bmatrix} \zeta & \mu \\ -\varepsilon & -\xi \end{bmatrix} \begin{bmatrix} E \\ H \end{bmatrix}. \tag{1.5}$$

For the two-dimensional photonic band structure, the electromagnetic transfer matrix method [8] is applied to the coupled system, similar to (1.5). For the 3D case, to the best of our knowledge no method has yet been proposed to solve the generalized eigenvalue problem (1.5) efficiently.

We make the following contributions to solve the discrete 3D generalized eigenvalue problem based on Yee's finite difference discretization scheme [32].

- We first derive the singular value decomposition (SVD) of the discrete single-curl operator $\nabla\times$ in (1.5).
- Using the SVD, we explore an explicit form of the basis for the invariant subspace corresponding to the nonzero eigenvalues of the GEP. Applying this basis, the GEP can be reduced to a null space free standard eigenvalue problem (NFSEP). In this eigenvalue problem, the zero eigenvalues of the GEP are deflated so that the null space does not degrade the computational efficiency.
- We show that all eigenvalues ω of the GEP are real provided the permittivity, permeability and magnetoelectric parameters satisfy particular assumptions. These assumptions are applicable to a couple of important classes of complex media.
- Under the same assumptions, we can reformulate the NFSEP as a null space free generalized eigenvalue problem $B_r x = \omega^{-1} A_r x$, where B_r is Hermitian and A_r is Hermitian positive definite. We demonstrate that this problem can be solved efficiently using the generalized Lanczos method algorithmically and numerically.

This paper is outlined as follows. In Section 2, we derive the singular value decomposition of the discrete single-curl operator. In Section 3, by applying the SVD, we derive a null space free eigenvalue problem by deflating the zero eigenvalues and keeping the nonzero eigenvalue unchanged. In Section 4, we discuss how to improve the solution performance while simulating two important types of complex media. In Section 5, we demonstrate numerical results to validate the correctness of proposed schemes and to measure the performance of the schemes. Finally, we present our conclusions in Section 6.

Throughout this paper, we use the superscripts $\top$ and $*$ to denote the transpose and the conjugate transpose of a matrix, respectively. For the matrix operations, we let $\otimes$ be the Kronecker product of two matrices. The imaginary number $\sqrt{-1}$ is written as i, and the identity matrix of dimension n is written as I_n.

2. Singular value decomposition of the discrete single-curl operator. In this section, we derive an explicit expression of the SVD of the discrete single-curl operator. Using this SVD, an efficient null space free method to solve the target eigenvalue problem (1.5) is developed in Section 3.

We start from the derivation of the matrix representation of the discrete single-curl operator. By using Yee's scheme [32], the discrete single-curl operators $\nabla \times E$ and $\nabla \times H$ with $\mathbf{a}_\ell = a\mathbf{e}_\ell$, $\ell = 1, 2, 3$ can be represented in the matrix form CE and

C^*H [13, 14], respectively. Here,

$$C = \begin{bmatrix} 0 & -C_3 & C_2 \\ C_3 & 0 & -C_1 \\ -C_2 & C_1 & 0 \end{bmatrix} \in \mathbb{C}^{3n\times 3n}, \tag{2.1}$$

with

$$C_1 = \delta_x^{-1}\left(I_{n_3}\otimes I_{n_2}\otimes K_{\mathbf{a}_1,n_1}\right) \in \mathbb{C}^{n\times n}, \tag{2.2a}$$
$$C_2 = \delta_y^{-1}\left(I_{n_3}\otimes K_{\mathbf{a}_2,n_2}\otimes I_{n_1}\right) \in \mathbb{C}^{n\times n}, \tag{2.2b}$$
$$C_3 = \delta_z^{-1}\left(K_{\mathbf{a}_3,n_3}\otimes I_{n_2}\otimes I_{n_1}\right) \in \mathbb{C}^{n\times n}, \tag{2.2c}$$

and

$$K_{\mathbf{a},m} = \begin{bmatrix} -1 & 1 & & \\ & \ddots & \ddots & \\ & & -1 & 1 \\ e^{\mathrm{i}2\pi\mathbf{k}\cdot\mathbf{a}} & & & -1 \end{bmatrix} \in \mathbb{C}^{m\times m}. \tag{2.3}$$

We use n_1, n_2, and n_3 to denote the numbers of grid points in the x, y, and z directions, respectively, and we define $n = n_1n_2n_3$. We use δ_x, δ_y, and δ_z to denote the associated mesh lengths along the x, y, and z axial directions, respectively.

It is worth noting that the divergence free conditions (1.1) and the quasi-periodicity conditions (1.2) are satisfied in Yee's scheme [14, Sections 5 and 3]. In addition to Yee's scheme, there are other approaches to deal with the quasi-periodicity conditions. First, the curl operators can be replaced by the shifted operator, so that the transformation of the solution leads to a periodic solution [9, 24, 34]. Second, we can use quasi-periodic basis funcitnos in finite element methods to resolve the quasi-periodicity conditions explicitly [25].

It is well known that the eigendecompositions of C^*C and CC^* are closely related to the SVD of C. Therefore, we start the derivation from the eigendecompositions of C^*C and CC^*. First, we introduce the notations to be used later. Define $\theta_{m,i} = \frac{\mathrm{i}2\pi i}{m}$, $\theta_{\mathbf{a},m} = \frac{\mathrm{i}2\pi\mathbf{k}\cdot\mathbf{a}}{m}$,

$$D_{\mathbf{a},m} = \operatorname{diag}\left(1, e^{\theta_{\mathbf{a},m}}, \cdots, e^{(m-1)\theta_{\mathbf{a},m}}\right), \tag{2.4}$$
$$\mathbf{u}_{m,i} = \begin{bmatrix} 1 & e^{\theta_{m,i}} & \cdots & e^{(m-1)\theta_{m,i}} \end{bmatrix}^\top$$

for $i = 0, \ldots, m-1$ and

$$U_m = \begin{bmatrix} \mathbf{u}_{m,0} & \cdots & \mathbf{u}_{m,m-1} \end{bmatrix} \in \mathbb{C}^{m\times m}, \tag{2.5}$$
$$\Lambda_{\mathbf{a},m} = \operatorname{diag}\begin{pmatrix} e^{\theta_{m,0}+\theta_{\mathbf{a},m}}-1 & \cdots & e^{\theta_{m,m-1}+\theta_{\mathbf{a},m}}-1 \end{pmatrix}. \tag{2.6}$$

By the definition of $K_{\mathbf{a},m}$ in (2.3), it can be verified that

$$K_{\mathbf{a},m}\left(D_{\mathbf{a},m}U_m\right) = \left(D_{\mathbf{a},m}U_m\right)\Lambda_{\mathbf{a},m}. \tag{2.7}$$

Denote

$$T = \frac{1}{\sqrt{n}}\left(D_{\mathbf{a}_3,n_3}\otimes D_{\mathbf{a}_2,n_2}\otimes D_{\mathbf{a}_1,n_1}\right)\left(U_{n_3}\otimes U_{n_2}\otimes U_{n_1}\right), \tag{2.8}$$

where $D_{\mathbf{a},n_i}$ and U_{n_i}, $i = 1, 2, 3$, are given in (2.4) and (2.5), respectively. It is straightforward to check that T is unitary. The following theorem which yields us the eigendecomposition of C_ℓ, for $\ell = 1, 2, 3$, can be proved with (2.7) and the property

$$(A_1 \otimes A_2 \otimes A_3)(B_1 \otimes B_2 \otimes B_3) = (A_1 B_1) \otimes (A_2 B_2) \otimes (A_3 B_3). \tag{2.9}$$

THEOREM 2.1. *C_1, C_2 and C_3 can be diagonalized by the unitary matrix T in the forms*

$$C_1 T = \delta_x^{-1} T \left(I_{n_3} \otimes I_{n_2} \otimes \Lambda_{\mathbf{a}_1,n_1}\right) \equiv T\Lambda_1, \tag{2.10a}$$
$$C_2 T = \delta_y^{-1} T \left(I_{n_3} \otimes \Lambda_{\mathbf{a}_2,n_2} \otimes I_{n_1}\right) \equiv T\Lambda_2, \tag{2.10b}$$
$$C_3 T = \delta_z^{-1} T \left(\Lambda_{\mathbf{a}_3,n_3} \otimes I_{n_2} \otimes I_{n_1}\right) \equiv T\Lambda_3. \tag{2.10c}$$

We now define two intermediate matrices Λ_p and Λ_q that are used in the eigendecompositions of C^*C and CC^*.

LEMMA 2.2. *Let Λ_1, Λ_2 and Λ_3 be given in* (2.10). *Define*

$$\Lambda_q = \Lambda_1^*\Lambda_1 + \Lambda_2^*\Lambda_2 + \Lambda_3^*\Lambda_3, \quad \Lambda_p = \begin{bmatrix} \beta\Lambda_3 - \Lambda_2 \\ \Lambda_1 - \alpha\Lambda_3 \\ \alpha\Lambda_2 - \beta\Lambda_1 \end{bmatrix} \tag{2.11}$$

with $\alpha, \beta \neq 0$. Assume that the vector $\mathbf{k} = (\mathrm{k}_1, \mathrm{k}_2, \mathrm{k}_3)^\top$ in (1.2) *is nonzero with $0 \leq \mathrm{k}_1, \mathrm{k}_2, \mathrm{k}_3 \leq \frac{1}{2}$. Then, Λ_q is positive definite, and Λ_p is of full column rank, provided that $\alpha\delta_x \neq \beta\delta_y$ and $\delta_z \neq \beta\delta_y$.*

Proof. See the appendix. □

Using the definitions of C and Λ_q in (2.1) and (2.11), respectively, and the eigendecompositions of C_ℓ in Theorem 2.1, the null spaces of C^*C and CC^* are derived as follows.

THEOREM 2.3. *Assume $\mathbf{k} = (\mathrm{k}_1, \mathrm{k}_2, \mathrm{k}_3)^\top \neq 0$ with $0 \leq \mathrm{k}_1, \mathrm{k}_2, \mathrm{k}_3 \leq \frac{1}{2}$. Define*

$$Q_0 = (I_3 \otimes T) \begin{bmatrix} \Lambda_1 \\ \Lambda_2 \\ \Lambda_3 \end{bmatrix} \Lambda_q^{-1/2} \equiv (I_3 \otimes T)\,\Pi_0, \quad P_0 = (I_3 \otimes T)\,\overline{\Pi_0}. \tag{2.12}$$

Then, Q_0 and P_0 form orthogonal bases of the null spaces of C^*C and CC^*, respectively.

Next, we apply the techniques developed in [11] to form the orthogonal bases for the range spaces of C^*C and CC^*. First, by considering the full column rank matrix $T_1 = [\alpha T^\top, \beta T^\top, T^\top]^\top$ with nonzero α and β, and taking the orthogonal projection of T_1 with respect to Q_0 and P_0, respectively, we have

$$\begin{aligned} Q_1 &= (I - Q_0 Q_0^*)\, T_1 \left(\Lambda_p^*\Lambda_p\Lambda_q^{-1}\right)^{-1/2} \\ &= (I_3 \otimes T) \begin{bmatrix} (\alpha\Lambda_2 - \beta\Lambda_1)\Lambda_2^* - (\Lambda_1 - \alpha\Lambda_3)\Lambda_3^* \\ (\beta\Lambda_3 - \Lambda_2)\Lambda_3^* - (\alpha\Lambda_2 - \beta\Lambda_1)\Lambda_1^* \\ (\Lambda_1 - \alpha\Lambda_3)\Lambda_1^* - (\beta\Lambda_3 - \Lambda_2)\Lambda_2^* \end{bmatrix} \left(\Lambda_p^*\Lambda_p\Lambda_q^{-1}\right)^{-1/2} \\ &\equiv (I_3 \otimes T)\,\Pi_1, \end{aligned} \tag{2.13a}$$

$$P_1 = (I - P_0 P_0^*)\, T_1 \left(\Lambda_p^*\Lambda_p\Lambda_q^{-1}\right)^{-1/2} = (I_3 \otimes T)\,\overline{\Pi_1}. \tag{2.13b}$$

Then, Q_1 and P_1 are orthogonal, and $(C^*C)Q_1 = Q_1\Lambda_q$ and $(CC^*)P_1 = P_1\Lambda_q$. Second, to form the remaining part of the orthogonal basis for the range spaces of C^*C and CC^*, we apply the discrete curl and dual-curl operators on T_1, respectively. That is, we pre-multiply C^* and C by T_1 to obtain

$$\begin{aligned} Q_2 &= C^*T_1\left(\Lambda_p^*\Lambda_p\right)^{-1/2} = (I_3\otimes T)\begin{bmatrix}\beta\Lambda_3^*-\Lambda_2^*\\ \Lambda_1^*-\alpha\Lambda_3^*\\ \alpha\Lambda_2^*-\beta\Lambda_1^*\end{bmatrix}\left(\Lambda_p^*\Lambda_p\right)^{-1/2} \\ &\equiv (I_3\otimes T)\,\Pi_2, \qquad (2.14a)\\ P_2 &= CT_1\left(\Lambda_p^*\Lambda_p\right)^{-1/2} = (I_3\otimes T)\left(-\overline{\Pi_2}\right). \qquad (2.14b)\end{aligned}$$

It holds that $(C^*C)Q_2 = Q_2\Lambda_q$ and $(CC^*)P_2 = P_2\Lambda_q$. From (2.12) to (2.14), we define

$$\begin{aligned} Q &\equiv \begin{bmatrix}Q_1 & Q_2 & Q_0\end{bmatrix} = (I_3\otimes T)\begin{bmatrix}\Pi_1 & \Pi_2 & \Pi_0\end{bmatrix}, \qquad (2.15a)\\ P &\equiv \begin{bmatrix}P_2 & P_1 & P_0\end{bmatrix} = (I_3\otimes T)\begin{bmatrix}-\overline{\Pi_2} & \overline{\Pi_1} & \overline{\Pi_0}\end{bmatrix}. \qquad (2.15b)\end{aligned}$$

Then, the eigendecompositions of C^*C and CC^* can be summarized as follows.

THEOREM 2.4. *Assume that the vector* $\mathbf{k} = (\mathrm{k}_1, \mathrm{k}_2, \mathrm{k}_3)^\top$ *in* (1.2) *is nonzero with* $0 \le \mathrm{k}_1, \mathrm{k}_2, \mathrm{k}_3 \le \frac{1}{2}$. *Then,* Q *and* P *are unitary, and*

$$C^*C = Q\,\mathrm{diag}\,(\Lambda_q, \Lambda_q, 0)\,Q^*, \quad CC^* = P\,\mathrm{diag}\,(\Lambda_q, \Lambda_q, 0)\,P^*. \qquad (2.16)$$

Motivated by (2.16), we derive the left and right singular vector matrices P and Q for C in the following theorem.

THEOREM 2.5 (Singular value decomposition of C). *Let* Λ_q *and* (Q, P) *be defined in* (2.11) *and* (2.15). *Assume that the vector* $\mathbf{k} = (\mathrm{k}_1, \mathrm{k}_2, \mathrm{k}_3)^\top$ *in* (1.2) *is nonzero with* $0 \le \mathrm{k}_1, \mathrm{k}_2, \mathrm{k}_3 \le \frac{1}{2}$. *Then, the matrix* C *in* (2.1) *has the SVD*

$$C = P\,\mathrm{diag}\left(\Lambda_q^{1/2}, \Lambda_q^{1/2}, 0\right)Q^* = P_r\Sigma_r Q_r^*, \qquad (2.17)$$

where

$$P_r = [P_2,\ P_1],\ Q_r = [Q_1,\ Q_2],\ \Sigma_r = \mathrm{diag}\left(\Lambda_q^{1/2}, \Lambda_q^{1/2}\right).$$

Proof. From (2.10) and the definition of C, it follows that

$$CT_1 = -(I_3\otimes T)\,\Lambda_p, \quad C^*T_1 = (I_3\otimes T)\,\overline{\Lambda_p}, \quad CQ_0 = 0, \text{ and } P_0^*C = 0. \qquad (2.18)$$

Combining (2.18) with (2.13) and (2.14), we have

$$\begin{aligned}
P_2^* C Q_1 &= \left(\Lambda_p^* \Lambda_p\right)^{-1/2} T_1^* C^* C \left(I - Q_0 Q_0^*\right) T_1 \left(\Lambda_p^* \Lambda_p \Lambda_q^{-1}\right)^{-1/2} \\
&= \left(\Lambda_p^* \Lambda_p\right)^{-1/2} T_1^* C^* C T_1 \left(\Lambda_p^* \Lambda_p \Lambda_q^{-1}\right)^{-1/2} = \Lambda_q^{1/2}, \\
P_1^* C Q_1 &= \left(\Lambda_p^* \Lambda_p \Lambda_q^{-1}\right)^{-1/2} T_1^* \left(I - P_0 P_0^*\right) C \left(I - Q_0 Q_0^*\right) T_1 \left(\Lambda_p^* \Lambda_p \Lambda_q^{-1}\right)^{-1/2} \\
&= \left(\Lambda_p^* \Lambda_p \Lambda_q^{-1}\right)^{-1/2} T_1^* C T_1 \left(\Lambda_p^* \Lambda_p \Lambda_q^{-1}\right)^{-1/2} \\
&= -\left(\Lambda_p^* \Lambda_p \Lambda_q^{-1}\right)^{-1/2} T_1^* \left(I_3 \otimes T\right) \Lambda_p \left(\Lambda_p^* \Lambda_p \Lambda_q^{-1}\right)^{-1/2} \\
&= -\left(\Lambda_p^* \Lambda_p \Lambda_q^{-1}\right)^{-1/2} \left(\begin{bmatrix} \alpha I & \beta I & I \end{bmatrix} \Lambda_p\right) \left(\Lambda_p^* \Lambda_p \Lambda_q^{-1}\right)^{-1/2} = 0, \\
P_1^* C Q_2 &= \left(\Lambda_p^* \Lambda_p \Lambda_q^{-1}\right)^{-1/2} T_1^* \left(I - P_0 P_0^*\right) C C^* T_1 \left(\Lambda_p^* \Lambda_p\right)^{-1/2} \\
&= \left(\Lambda_p^* \Lambda_p \Lambda_q^{-1}\right)^{-1/2} T_1^* C C^* T_1 \left(\Lambda_p^* \Lambda_p\right)^{-1/2} = \Lambda_q^{1/2}, \\
P_2^* C Q_2 &= \left(\Lambda_p^* \Lambda_p\right)^{-1/2} T_1^* C^* C Q_2 = \left(\Lambda_p^* \Lambda_p\right)^{-1/2} T_1^* Q_2 \Lambda_q \\
&= \left(\Lambda_p^* \Lambda_p\right)^{-1/2} T_1^* C^* T_1 \left(\Lambda_p^* \Lambda_p\right)^{-1/2} \Lambda_q = 0.
\end{aligned}$$

Therefore, we obtain the SVD of C described in (2.17). □

Now, we consider the case that $\mathbf{k} = \mathbf{0}$ in Lemma 2.6 and Theorem 2.7. Note that, in this case, the GEP (1.5) has $n+2$ zero eigenvalues [13].

LEMMA 2.6. *If $\mathbf{k} = \mathbf{0}$, then Λ_q and Λ_p in (2.11) have rank $n-1$. Furthermore, $\Lambda_q(1,1) = 0$ and the first column of Λ_p is a zero vector.*

Proof. If $\mathbf{k} = 0$, it holds that $\Lambda_{a,m}(1,1) = 0$ and $\Lambda_{a,m}(i,i) \neq 0$ for $i \neq 1$ by (2.6). This fact implies that $\Lambda_1(1,1) = \Lambda_2(1,1) = \Lambda_3(1,1) = 0$ in (2.10). Therefore, by the definitions of Λ_q and Λ_p in (2.11), Λ_q and Λ_p have rank $n-1$ and the first columns of Λ_q and Λ_p are zero vectors. □

We define two notations that are used in the following theorem. For a given a matrix $F \in \mathbb{C}^{n\times n}$, let $F_c \in \mathbb{C}^{n\times(n-1)}$ (or $F_{rc} \in \mathbb{C}^{(n-1)\times(n-1)}$) be the submatrices of F that the first column is deleted (or both the first column and the first row are deleted). Combining the results in Theorem 2.5 and Lemma 2.6, the singular value decomposition of C with $\mathbf{k} = 0$ can be obtained in Theorem 2.7.

THEOREM 2.7. *Let T, $(\Lambda_1, \Lambda_2, \Lambda_3)$ and (Λ_q, Λ_p) be defined in (2.8), (2.10) and (2.11), respectively. Assume $\mathbf{k} = \mathbf{0}$. Then*

$$C = \widehat{P}_r \widehat{\Sigma}_r \widehat{Q}_r^*,$$

where

$$\begin{aligned}
&\widehat{Q}_r = \left(I_3 \otimes T\right) \begin{bmatrix} \Pi_{1,c} & \Pi_{2,c} \end{bmatrix}, \quad \widehat{P}_r = \left(I_3 \otimes T\right) \begin{bmatrix} -\overline{\Pi_{2,c}} & \overline{\Pi_{1,c}} \end{bmatrix}, \\
&\widehat{\Sigma}_r = \operatorname{diag}\left((\Lambda_q)_{rc}^{1/2}, (\Lambda_q)_{rc}^{1/2}\right)
\end{aligned}$$

with

$$\begin{aligned}
\Pi_{1,c} &= \begin{bmatrix} ((\alpha\Lambda_2 - \beta\Lambda_1)\Lambda_2^* - (\Lambda_1 - \alpha\Lambda_3)\Lambda_3^*)_c \\ ((\beta\Lambda_3 - \Lambda_2)\Lambda_3^* - (\alpha\Lambda_2 - \beta\Lambda_1)\Lambda_1^*)_c \\ ((\Lambda_1 - \alpha\Lambda_3)\Lambda_1^* - (\beta\Lambda_3 - \Lambda_2)\Lambda_2^*)_c \end{bmatrix} \left((\Lambda_p^*\Lambda_p)_{rc} (\Lambda_q)_{rc}^{-1}\right)^{-1/2}, \\
\Pi_{2,c} &= \begin{bmatrix} (\beta\Lambda_3^* - \Lambda_2^*)_c \\ (\Lambda_1^* - \alpha\Lambda_3^*)_c \\ (\alpha\Lambda_2^* - \beta\Lambda_1^*)_c \end{bmatrix} \left((\Lambda_p^*\Lambda_p)_{rc}\right)^{-1/2}.
\end{aligned}$$

It is worth mentioning the specific choice of the singular vector matrices P and Q in (2.15). The choice of these matrices is not unique because the multiplicities of the nonzero eigenvalues of C^*C are even and may be large. We have carefully chosen the P and Q defined in (2.15) to avoid the need to store these two matrices and the computations involving P and Q can be performed efficiently. We discuss this computational advantage in Section 4.2.

3. The null space free eigenvalue problem. We have derived the SVD of C in Theorem 2.5. In this section, we use the SVD to deflate the null space of the GEP obtained by discretizing (1.5) so that we can develop a new solution process for the target eigenvalue problem. The discretization of (1.5) based on Yee's scheme leads to the following discrete GEP

$$\begin{bmatrix} C & 0 \\ 0 & C^* \end{bmatrix} \begin{bmatrix} E \\ H \end{bmatrix} = \omega \left(\mathrm{i} \begin{bmatrix} \zeta_d & \mu_d \\ -\varepsilon_d & -\xi_d \end{bmatrix} \right) \begin{bmatrix} E \\ H \end{bmatrix}. \tag{3.1}$$

Here, C is the discrete single-curl operator defined in (2.1). The four $3n \times 3n$ complex matrices ζ_d, ξ_d, ε_d, μ_d are the discrete counterparts of the matrices ζ, ξ, ε and μ, respectively.

From Theorem 2.5, we can see that the GEP (3.1) has $2n$ zero eigenvalues. This null space not only affects the convergence of iterative eigensolvers but also increases the challenge of solving the eigenvalue problem. In this section, we apply the SVD of C in (2.17) to reduce the GEP (3.1) to the null space free eigenvalue problem (3.6) equipped with the following two advantages. (i) The dimension of the coefficient matrix is dramatically reduced from $6n$ in (3.1) to $4n$ in (3.6). (ii) The two eigenvalue problems share the same $4n$ nonzero eigenvalues.

To derive the NFSEP, we first rewrite (3.1) as

$$\mathrm{diag}\,(P_r, Q_r)\ \mathrm{diag}\,(\Sigma_r, \Sigma_r)\ \mathrm{diag}\,(Q_r^*, P_r^*) \begin{bmatrix} E \\ H \end{bmatrix} = \omega \left(\mathrm{i} \begin{bmatrix} \zeta_d & \mu_d \\ -\varepsilon_d & -\xi_d \end{bmatrix} \right) \begin{bmatrix} E \\ H \end{bmatrix} \tag{3.2}$$

by applying the SVD of C described in (2.17). We can then explicitly define the invariant subspace of (3.1) in the following theorem using the matrices P_r, Q_r, and Σ_r defined in Theorem 2.5.

THEOREM 3.1. *Assume the matrix*

$$B \equiv \mathrm{i} \begin{bmatrix} \zeta_d & \mu_d \\ -\varepsilon_d & -\xi_d \end{bmatrix} \tag{3.3}$$

is nonsingular. Then

$$\mathrm{span} \left\{ B^{-1}\, diag \left(P_r \Sigma_r^{\frac{1}{2}}, Q_r \Sigma_r^{\frac{1}{2}} \right) \right\}$$

is an invariant subspace of (3.1) *corresponding to all nonzero eigenvalues. Furthermore, it holds that*

$$\begin{aligned} &\left\{ \omega \,\middle|\, \mathrm{diag} \left(\Sigma_r^{\frac{1}{2}} Q_r^*, \Sigma_r^{\frac{1}{2}} P_r^* \right) B^{-1}\, \mathrm{diag} \left(P_r \Sigma_r^{\frac{1}{2}}, Q_r \Sigma_r^{\frac{1}{2}} \right) y = \omega y \right\} \\ &= \left\{ \omega \,|\, \mathrm{diag}\,(C, C^*)\, x = \omega B x,\ \omega \neq 0 \right\}. \end{aligned} \tag{3.4}$$

Proof. From Theorem 2.5, we have

$$\begin{aligned}
&\operatorname{diag}(C, C^*)\left\{B^{-1}\operatorname{diag}\left(P_r\Sigma_r^{\frac{1}{2}}, Q_r\Sigma_r^{\frac{1}{2}}\right)\right\} \\
=\ &\left\{\operatorname{diag}\left(P_r\Sigma_r Q_r^*, Q_r\Sigma_r P_r^*\right)\right\}\left\{B^{-1}\operatorname{diag}\left(P_r\Sigma_r^{\frac{1}{2}}, Q_r\Sigma_r^{\frac{1}{2}}\right)\right\} \\
=\ &B\left\{B^{-1}\operatorname{diag}\left(P_r\Sigma_r^{\frac{1}{2}}, Q_r\Sigma_r^{\frac{1}{2}}\right)\right\}\left\{\operatorname{diag}\left(\Sigma_r^{\frac{1}{2}}Q_r^*, \Sigma_r^{\frac{1}{2}}P_r^*\right)B^{-1}\operatorname{diag}\left(P_r\Sigma_r^{\frac{1}{2}}, Q_r\Sigma_r^{\frac{1}{2}}\right)\right\}.
\end{aligned} \tag{3.5}$$

From (3.2), (3.5), and the fact that $\operatorname{diag}\left(\Sigma_r^{\frac{1}{2}}Q_r^*, \Sigma_r^{\frac{1}{2}}P_r^*\right)B^{-1}\operatorname{diag}\left(P_r\Sigma_r^{\frac{1}{2}}, Q_r\Sigma_r^{\frac{1}{2}}\right) \in \mathbb{C}^{4n\times 4n}$ is nonsingular, we can see that $\operatorname{span}\{B^{-1}\operatorname{diag}\left(P_r\Sigma_r^{\frac{1}{2}}, Q_r\Sigma_r^{\frac{1}{2}}\right)\}$ is an invariant subspace of the GEP (3.1) corresponding to all nonzero eigenvalues, and therefore the result in (3.4) holds. ∎

From Theorem 3.1, the null space free eigenvalue problem is derived straightforwardly in the following theorem.

THEOREM 3.2 (The null space free eigenvalue problem). *For any nonsingular B defined in* (3.3)*, the GEP* (3.1) *can be reduced to the following null space free eigenvalue problem*

$$\operatorname{diag}\left(\Sigma_r^{\frac{1}{2}}Q_r^*, \Sigma_r^{\frac{1}{2}}P_r^*\right)B^{-1}\operatorname{diag}\left(P_r\Sigma_r^{\frac{1}{2}}, Q_r\Sigma_r^{\frac{1}{2}}\right)y = \omega y. \tag{3.6}$$

Furthermore, the GEP (3.1) *and the NFSEP* (3.6) *have the same nonzero eigenvalues.*

We have reduced the GEP (3.1) to the NFSEP (3.6), and the NFSEP can be solved by the iterative eigensolvers without being disturbed by the null space. Further computational considerations are discussed in the next section. Finally, we note how the $\mathbb{C}^{3n\times 3n}$ matrices ζ_d, ξ_d, ε_d, and μ_d are determined. In Yee's scheme, E and H are evaluated at the edge centers and the face centers, respectively. However, CE and C^*H are evaluated at the face centers and the edge centers, respectively. To match these evaluation points, we can average the corresponding discrete entry values of ζ, ξ, ε and μ on the neighbor grid points to form the matrices ζ_d, ξ_d, ε_d, μ_d in (3.1). Consequently, $\zeta_d E + \mu_d H$ and $\varepsilon_d E + \xi_d H$ are evaluated at the face centers and the edge centers, respectively.

4. Computational and application considerations. The NFSEP defined in (3.6) can actually be applied to various complex media settings as long as the corresponding matrix B is nonsingular. Such media include general and Tellegen biisotropic media [30], lossless and reciprocal bianisotropic media [26], and general bianisotropic media [16]. To solve the NFSEP, shift-and-invert type iterative eigensolvers (e.g., Arnoldi method, Jacobi-Davidson method) can be applied to compute the desired eigenpairs of (3.1) from (3.6) without being affected by zero eigenvalues. Despite the wide applications on complex media, the process for solving the NFSEP (3.6) can be further accelerated under the mild assumption described in Section 4.1. It is worth mentioning that two important types of media, i.e., chiral media [3, 4, 21, 27, 30, 33] and pseudochiral media [2, 5, 6, 16, 28], satisfy this assumption and can thus be solved by the accelerated eigensolvers. See Sections 4.2 and 4.3 for more details and some computational remarks.

4.1. Sufficient conditions for Hermitian and Hermitian positive definite generalized eigenvalue problems. The coefficient matrix in the NFSEP (3.6) is

in a general form, and the NFSEP can therefore be solved using, for example, the Arnoldi method. However, under an assumption, we can rewrite the NFSEP (3.6) as a generalized eigenvalue problem with Hermitian and Hermitian positive definite coefficient matrices. We can then take advantage of the matrix structure to accelerate the solution process by solving this rewritten eigenvalue problem via the invert Lanczos method and the associated conjugate gradient linear system solver.

The acceleration scheme is motivated from the following observations regarding the matrix B in (3.3). If μ_d is nonsingular and we let Φ represent the matrix $\varepsilon_d - \xi_d\mu_d^{-1}\zeta_d$, we have

$$B = \mathrm{i}\begin{bmatrix} 0 & \mu_d \\ -\Phi & -\xi_d \end{bmatrix}\begin{bmatrix} I_{3n} & 0 \\ \mu_d^{-1}\zeta_d & I_{3n} \end{bmatrix}.$$

Furthermore, if Φ is nonsingular, we have

$$B^{-1} = -\mathrm{i}\begin{bmatrix} I_{3n} & 0 \\ -\mu_d^{-1}\zeta_d & I_{3n} \end{bmatrix}\begin{bmatrix} -\Phi^{-1}\xi_d\mu_d^{-1} & -\Phi^{-1} \\ \mu_d^{-1} & 0 \end{bmatrix}. \tag{4.1}$$

In other words, the properties of B^{-1} are closely related to μ_d, Φ, ξ_d and ζ_d. In particular, we consider the assumption

$$\mu_d \succ 0, \Phi \equiv \varepsilon_d - \xi_d\mu_d^{-1}\zeta_d \succ 0, \text{ and } \xi_d^* = \zeta_d. \tag{4.2}$$

The notations $\mu_d \succ 0$ and $\Phi \succ 0$ suggest that μ_d and Φ are Hermitian positive definite. Under this assumption, we show that the GEP (3.1) can be transformed to a standard Hermitian eigenvalue problem (so that all of the eigenvalues are real) in Theorem 4.1. We then rewrite the NFSEP (3.6) in the new form (4.9) in Theorem 4.2. Consequently, the corresponding coefficient matrix A_r to be defined in (4.10) is Hermitian and positive definite. We can then use the Lanczos method, which consumes less storage and computation than Arnoldi-type methods, to solve (4.9).

We begin the derivation from the following theorem.

THEOREM 4.1. *Under Assumption* (4.2)*, all eigenvalues* ω *of the GEP* (3.1) *are real.*

Proof. Let

$$\begin{bmatrix} E_\zeta \\ H_\zeta \end{bmatrix} = \begin{bmatrix} I_{3n} & 0 \\ \mu_d^{-1}\zeta_d & I_{3n} \end{bmatrix}\begin{bmatrix} E \\ H \end{bmatrix}. \tag{4.3}$$

Substituting (4.3) into (3.1) and pre-multiplying (3.1) by $\begin{bmatrix} I_{3n} & 0 \\ \xi_d\mu_d^{-1} & I_{3n} \end{bmatrix}$, it holds that

$$\begin{bmatrix} C & 0 \\ \xi_d\mu_d^{-1}C - C^*\mu_d^{-1}\zeta_d & C^* \end{bmatrix}\begin{bmatrix} E_\zeta \\ H_\zeta \end{bmatrix} = \mathrm{i}\omega\begin{bmatrix} 0 & \mu_d \\ -\Phi & 0 \end{bmatrix}\begin{bmatrix} E_\zeta \\ H_\zeta \end{bmatrix}, \tag{4.4}$$

where Φ is defined in Assumption (4.2). By the assumptions that $\mu_d \succ 0$ and $\Phi \succ 0$, we then let

$$\mu_d = \mu_c\mu_c^*, \quad \Phi = \Phi_c\Phi_c^* \tag{4.5}$$

be the Cholesky decompositions of μ_d and Φ, respectively. Define

$$\begin{bmatrix} \widetilde{E} \\ \widetilde{H} \end{bmatrix} = \begin{bmatrix} \Phi_c^* & 0 \\ 0 & \mu_c^* \end{bmatrix}\begin{bmatrix} E_\zeta \\ H_\zeta \end{bmatrix}. \tag{4.6}$$

Substituting (4.6) into (4.4) and pre-multiplying (4.4) by $\begin{bmatrix} 0 & -\Phi_c^{-1} \\ \mu_c^{-1} & 0 \end{bmatrix}$, we have

$$Ax = \omega x, \tag{4.7}$$

where $x = [\widetilde{E}^\top,\ \widetilde{H}^\top]^\top$ and

$$A = (-\mathrm{i}) \begin{bmatrix} -\Phi_c^{-1} \left(\xi_d \mu_d^{-1} C - C^* \mu_d^{-1} \zeta_d\right) \left(\Phi_c^*\right)^{-1} & -\Phi_c^{-1} C^* \left(\mu_c^*\right)^{-1} \\ \mu_c^{-1} C \left(\Phi_c^*\right)^{-1} & 0 \end{bmatrix}. \tag{4.8}$$

Because A is Hermitian, all eigenvalues ω of the GEP (3.1) are real. □

We have shown that all eigenvalues of (3.1) are real under Assumption (4.2). However, the coefficient matrix of the NFSEP in (3.6) is not Hermitian. We reformulate the NFSEP (3.6) in the following theorem to obtain a Hermitian and Hermitian positive definite generalized eigenvalue problem (HHPD-GEP).

THEOREM 4.2. *Under Assumption* (4.2)*, the GEP* (3.1) *can be reduced to a null space free generalized eigenvalue problem*

$$\left(\mathrm{i} \begin{bmatrix} 0 & \Sigma_r^{-1} \\ -\Sigma_r^{-1} & 0 \end{bmatrix}\right) y_r = \omega^{-1} A_r y_r, \tag{4.9}$$

where

$$A_r \equiv \operatorname{diag}\left(P_r^*, Q_r^*\right) \begin{bmatrix} \mu_d^{-1}\zeta_d & -I_{3n} \\ I_{3n} & 0 \end{bmatrix} \begin{bmatrix} \Phi^{-1} & 0 \\ 0 & \mu_d^{-1} \end{bmatrix} \begin{bmatrix} \xi_d \mu_d^{-1} & I_{3n} \\ -I_{3n} & 0 \end{bmatrix} \operatorname{diag}\left(P_r, Q_r\right) \tag{4.10}$$

is Hermitian and positive definite.

Proof. Let

$$y_r = \operatorname{diag}\left(\Sigma_r^{1/2}, \Sigma_r^{1/2}\right) y.$$

Rewrite (3.6) as

$$\operatorname{diag}\left(Q_r^*, P_r^*\right) B^{-1} \operatorname{diag}\left(P_r, Q_r\right) y_r = \omega \operatorname{diag}\left(\Sigma_r^{-1}, \Sigma_r^{-1}\right) y_r,$$

which is equivalent to

$$\mathrm{i} \operatorname{diag}\left(P_r^*, Q_r^*\right) \begin{bmatrix} 0 & I_{3n} \\ -I_{3n} & 0 \end{bmatrix} B^{-1} \operatorname{diag}\left(P_r, Q_r\right) y_r = \omega \left(\mathrm{i} \begin{bmatrix} 0 & \Sigma_r^{-1} \\ -\Sigma_r^{-1} & 0 \end{bmatrix}\right) y_r. \tag{4.11}$$

From (4.1), it holds that

$$\begin{aligned} \mathrm{i} \begin{bmatrix} 0 & I_{3n} \\ -I_{3n} & 0 \end{bmatrix} B^{-1} &= \begin{bmatrix} \mu_d^{-1}\zeta_d & -I_{3n} \\ I_{3n} & 0 \end{bmatrix} \begin{bmatrix} \Phi^{-1}\xi_d\mu_d^{-1} & \Phi^{-1} \\ -\mu_d^{-1} & 0 \end{bmatrix} \\ &= \begin{bmatrix} \mu_d^{-1}\zeta_d & -I_{3n} \\ I_{3n} & 0 \end{bmatrix} \begin{bmatrix} \Phi^{-1} & 0 \\ 0 & \mu_d^{-1} \end{bmatrix} \begin{bmatrix} \xi_d\mu_d^{-1} & I_{3n} \\ -I_{3n} & 0 \end{bmatrix}, \end{aligned}$$

which is Hermitian and positive definite if Assumption (4.2) holds. That is, the coefficient matrix on the left hand side of (4.11) is equal to A_r. Therefore, the equation (4.11) can be rewritten as (4.9). □

We have now asserted the sufficient conditions that lead to the Hermitian and Hermitian positive definite null space free generalized eigenvalue problem (HHPD-NFGEP) (4.9). Next, we discuss some considerations in applying and solving the HHPD-NFGEP.

4.2. The eigenvalue and associated linear system solvers. In the HHPD-NFGEP (4.9), the coefficient matrix A_r is Hermitian and positive definite. We can use the generalized Lanczos method to solve (4.9) and obtain the smallest positive eigenvalues that are of interest in complex media. In each step of the generalized Lanczos method, we must solve the linear systems

$$A_r u \equiv \begin{bmatrix} P_r^* & \\ & Q_r^* \end{bmatrix} \begin{bmatrix} \zeta_d & -I_{3n} \\ I_{3n} & 0 \end{bmatrix} \begin{bmatrix} \Phi^{-1} & 0 \\ 0 & I_{3n} \end{bmatrix} \begin{bmatrix} \zeta_d^* & I_{3n} \\ -I_{3n} & 0 \end{bmatrix} \begin{bmatrix} P_r & \\ & Q_r \end{bmatrix} u = b \qquad (4.12)$$

for a given vector b. Because A_r is Hermitian positive definite, the linear system (4.12) can be solved efficiently by using the conjugate gradient method. Furthermore, the matrix-vector multiplications of the forms $(T^*\mathbf{p}, T\mathbf{q})$ for computing $(P_r^*\hat{\mathbf{p}}_1, Q_r^*\hat{\mathbf{p}}_2)$ and $(P_r\hat{\mathbf{q}}_1, Q_r\hat{\mathbf{q}}_2)$, which are the most costly parts of solving (4.12), can be computed efficiently by the 3D FFT because of the periodicity of T, as shown in (2.8).

4.3. Application remarks. Intensive research has been conducted on chiral and pseudochiral media. In this section, we assert that the corresponding magnetoelectric matrices satisfy the assumptions given in (4.2), and we can therefore solve the HHPD-NFGEP using the Lanczos method. This solution procedure can thus act as a useful numerical tool for simulating 3D chiral and pseudochiral media.

First, we introduce the magnetoelectric matrices in chiral and pseudochiral media. For chiral media (also called Pasteur or reciprocal chiral media), the associated magnetoelectric matrices ζ_d and ξ_d in (3.1) are of the forms

$$\xi_d = \mathrm{i}\gamma\tilde{I}_{3n} \text{ and } \zeta_d = -\mathrm{i}\gamma\tilde{I}_{3n}. \qquad (4.13)$$

Here, γ is the chirality parameter, and $\tilde{I}_m \in \mathbb{R}^{m\times m}$ is a diagonal matrix whose entries are equal to 0 (outside of the medium) or 1 (within the medium) depending on the corresponding grid point locations. For pseudochiral media, the associated matrices are

$$\xi_d = \begin{bmatrix} 0 & 0 & \mathrm{i}\gamma\tilde{I}_n \\ 0 & 0 & 0 \\ \mathrm{i}\gamma\tilde{I}_n & 0 & 0 \end{bmatrix} \text{ and } \zeta_d = \begin{bmatrix} 0 & 0 & -\mathrm{i}\gamma\tilde{I}_n \\ 0 & 0 & 0 \\ -\mathrm{i}\gamma\tilde{I}_n & 0 & 0 \end{bmatrix}. \qquad (4.14)$$

Now, we analyze these magnetoelectric matrices. For chiral and pseudochiral media, ε are of the form of 3-by-3 diagonal block matrix that $\varepsilon = \mathrm{diag}(\epsilon, \epsilon, \epsilon)$. Here, ϵ is a piecewise constant function that is equal to ε_i and ε_o inside and outside the medium, respectively. Thus, the associated matrix ε_d in (3.1) is a diagonal matrix with ε_o or ε_i on diagonal entries. On the other hand, the permeability μ is usually taken as I_3, so the matrix μ_d in (3.1) is equal to an identity. Combining the diagonal matrices ε_d and μ_d with (ξ_d, ζ_d) in (4.13) and (4.14), we have that $\Phi = \varepsilon_d - \xi_d\mu_d^{-1}\zeta_d = \varepsilon_d - \xi_d\zeta_d$ is a diagonal matrix with the entries ε_o, ε_i, or $\varepsilon_i - \gamma^2$. Because ε_o and ε_i are positive, Φ is a positive diagonal matrix, provided $\gamma \in (0, \sqrt{\varepsilon_i})$.

4.4. A short summary. In Table 4.1, we summarize all of the eigenvalue problems and eigensolver strategies that have been discussed in the previous sections. From the algorithmic viewpoint, we propose and outline the Null Space Free method (NSF) in Algorithm 1.

5. Numerical results. In the numerical experiments, we consider 3D reciprocal chiral materials, in which $\zeta = -\mathrm{i}\gamma$. The goals of our numerical experiments are

(a)	GEP (1.5)	NFSEP (3.6)	HSEP (4.7)	HHPD-NFGEP (4.2)
(b)	Generalized non-Hermitian	Standard non-Hermitian	Standard Hermitian	Generalized Hermitian & HPD
(c)	Complex	Complex	Real (Thm. 4.1)	Real
(d)	$6n \times 6n$	$4n \times 4n$	$6n \times 6n$	$4n \times 4n$
(e)	$2n$ (Thm. 2.5)	0 (Thm. 3.2)	$2n$	0
(f)	S.I. Arnoldi	S.I. Arnoldi	S.I. Lanczos	S.I. Lanczos
(g)	Hard to choose	Zero	Hard to choose	Zero
(h)	(5.1)	-	-	(4.12)
(i)	LU or GMRES (not efficient)	-	-	CG with FFT Mtx-Vec Mult.
(j)	Hard to find	None (well-cond.)	Harder to find	None (well-cond.)
(k)	Media without Assum. (4.2)	Media without Assum. (4.2)	Media without Assum. (4.2)	Media satisfying Assum. (4.2) (Thm. 4.2)

TABLE 4.1

A summary of the eigenvalue problems and solvers considered in this article. The table lists (a) names of the eigenvalue problems, (b) type of the eigenvalue problems, (c) type of eigenvalues, (d) problem dimensions, (e) number of zero eigenvalues, (f) eigenvalue solver, (g) choice of shift σ for the smallest eigenvalues, (h) embedded linear systems, (i) linear system solvers, (j) preconditioners for the linear system solvers, and (k) the applicable complex media.

FIG. 5.1. *A schema of 3D chiral medium with a simple cubic lattice within a single primitive cell.*

threefold: to verify the correctness of the proposed algorithms and the code implementation, to compare the performance of the proposed algorithm with an existing algorithm, and to study the performance of the proposed method in terms of iteration numbers and execution time. The details of the numerical experiments are as follows.

For the medium structure, we consider a simple cubic lattice consisting of spheres with radius r and circular cylinders with radius s, as shown in Figure 5.1. In par-

Algorithm 1 The null space free method (NSF) for solving the GEP (3.1)

1: Compute Λ_1, Λ_2 and Λ_3 in Theorem 2.1;
2: Compute Λ_q and Λ_p in (2.11);
3: Compute Π_1 and Π_2 in (2.13a) and (2.14a), respectively;
4: **if** μ_d and Φ are Hermitian positive definite and $\xi_d^* = \zeta_d$ **then**
5: Solve the HHPD-NFGEP

$$\left(\mathrm{i}\begin{bmatrix} 0 & \Sigma_r^{-1} \\ -\Sigma_r^{-1} & 0 \end{bmatrix}\right) y = \omega^{-1} A_r y,$$

where A_r is defined in (4.10);
6: **else**
7: Solve the NFSEP

$$\mathrm{diag}\left(\Sigma_r^{1/2} Q_r^*, \Sigma_r^{1/2} P_r^*\right) B^{-1} \mathrm{diag}\left(P_r \Sigma_r^{1/2}, Q_r \Sigma_r^{1/2}\right) y = \omega y.$$

8: Update $y = \mathrm{diag}\left(\Sigma_r^{1/2}, \Sigma_r^{1/2}\right) y$;
9: **end if**
10: Compute

$$x = B^{-1} \mathrm{diag}\left(P_r, Q_r\right) y.$$

ticular, we assume the lattice constant $a = 1$, $r/a = 0.345$, and $s/a = 0.11$. We use the triplet $(\varepsilon_i, \varepsilon_o, \gamma)$ to represent the associated permittivity inside the structure, the permittivity outside the structure, and the chirality parameter, respectively. The perimeter of the irreducible Brillouin zone for the sample cubic lattice is formed by the corners $G = [0,0,0]^\top$, $X = \frac{2\pi}{a}\left[\frac{1}{2}, 0, 0\right]^\top$, $M = \frac{2\pi}{a}\left[\frac{1}{2}, \frac{1}{2}, 0\right]^\top$, and $R = \frac{2\pi}{a}\left[\frac{1}{2}, \frac{1}{2}, \frac{1}{2}\right]^\top$.

For the implementation, the MATLAB function `eigs` is used to solve the HHPD-NFGEP (4.9), and `pcg` (without preconditioning) is used to solve the associated linear system (4.12). The stopping criteria for `eigs` and `pcg` are $10^4 \times \epsilon/(2\sqrt{\delta_x^{-2} + \delta_y^{-2} + \delta_z^{-2}})$ and 10^{-14}, respectively. The constant ϵ ($\approx 2.2 \times 10^{-16}$) is the floating-point relative accuracy in MATLAB. In `eigs`, the maximal number of Lanczos vectors for the restart is 3ℓ, where $\ell = 10$ is the number of desired eigenvalues of the GEP (3.1). The MATLAB functions `fftn` and `ifftn` are applied to compute the matrix-vector products $T^*\mathbf{p}$ and $T\mathbf{q}$, respectively. The MATLAB commands `tic` and `toc` are used to measure the elapsed time. All computations are performed in MATLAB 2011b.

For the hardware configuration, we use a HP workstation equipped with two Intel Quad-Core Xeon X5687 3.6GHz CPUs, 48 GB of main memory, and RedHat Linux operating system Version 5.

5.1. Numerical correctness validation. We validate the correctness of the proposed algorithm and MATLAB implementation by solving the following three sets of benchmark problems.

First, we consider a special case $(\varepsilon_i, \varepsilon_o, \gamma) = (13, 1, 0)$, whose corresponding band structure have been reported in [7, 10, 13, 20]. In this case, because of $\gamma = 0$ and (1.4a), we can see that the GEP (3.1) and the eigenvalue problem $AE = \omega^2 \varepsilon_d E$ (for the photonic crystal as shown in [13]) lead to the same band structure. The computed

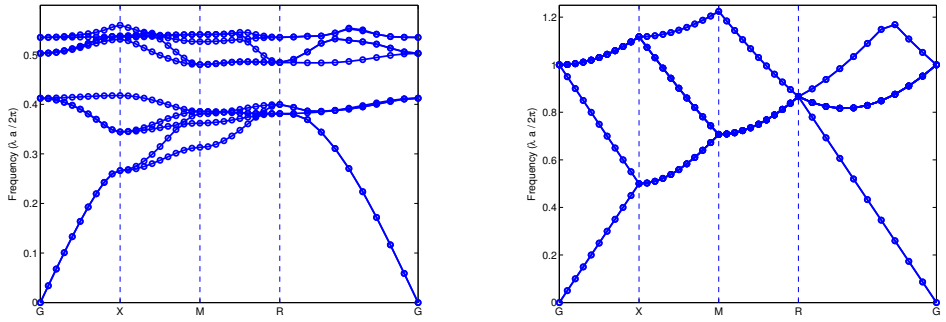

(a) $(\varepsilon_i, \varepsilon_o, \gamma) = (13, 1, 0)$ (b) $(\varepsilon_i, \varepsilon_o, \gamma) = (1, 1, 0)$

FIG. 5.2. *The band structure with* $(\varepsilon_i, \varepsilon_o, \gamma) = (13, 1, 0)$ *and* $(1, 1, 0)$.

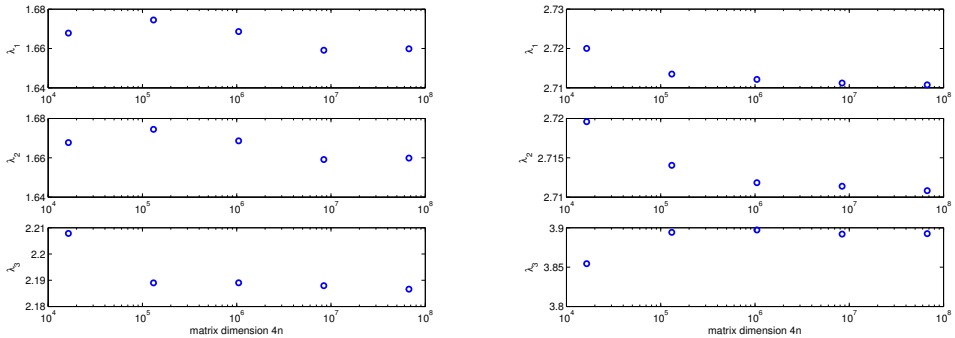

(a) $(\varepsilon_i, \varepsilon_o, \gamma) = (13, 1, 0.5)$ (b) $(\varepsilon_i, \varepsilon_o, \gamma) = (1, 1, 0.8)$

FIG. 5.3. *The convergent eigenvalues for* $(\varepsilon_i, \varepsilon_o, \gamma) = (13, 1, 0.5)$ *and* $(\varepsilon_i, \varepsilon_o, \gamma) = (1, 1, 0.8)$ *with various matrix sizes* $4n$.

band structure due to (3.1) and $n_1 = n_2 = n_3 = 50$ is shown in Figure 5.2(a). The figure is identical (up to numerical precision) to Figure 1(a) in [13].

Second, we consider $(\varepsilon_i, \varepsilon_o, \gamma) = (1, 1, 0)$, for which some theoretical results are known. In this case, we know that (3.1) and $AE = \omega^2 E$ have the same band structure and, from Theorem 2.4, $\{\Lambda_q, \Lambda_q\}$ are the nonzero eigenvalues of A. That is, $\{\Lambda_q^{1/2}, \Lambda_q^{1/2}\}$ are the eigenvalues of (3.1). Comparing the computed eigenvalues shown in Figure 5.2(b) (for $n_1 = n_2 = n_3 = 50$) with the exact eigenvalues, our numerical results show that the maximal relative error of all computed eigenvalues in the figure is 3.65×10^{-14}.

Third, we check the convergence of the eigenvalues in terms of the grid point numbers. In particular, we set $n_1 = n_2 = n_3 = 2^k$ for $k = 3, \ldots, 7$, and the corresponding matrix sizes $4n = 4 \times 2^{3k}$ of the NFSEP (4.9) range from $2,048$ to $8,388,608$. The three smallest positive eigenvalues $\lambda_{1,k}$, $\lambda_{2,k}$ and $\lambda_{3,k}$ for $(\varepsilon_i, \varepsilon_o, \gamma) = (13, 1, 0.5)$ and $(\varepsilon_i, \varepsilon_o, \gamma) = (1, 1, 0.8)$ are shown in Figure 5.3 for the wave vector $\mathbf{k} = [0.5, 0, 0]^\top$. The figure shows that $\{\lambda_{1,k}\}$, $\{\lambda_{2,k}\}$ and $\{\lambda_{3,k}\}$ are convergent as k increases.

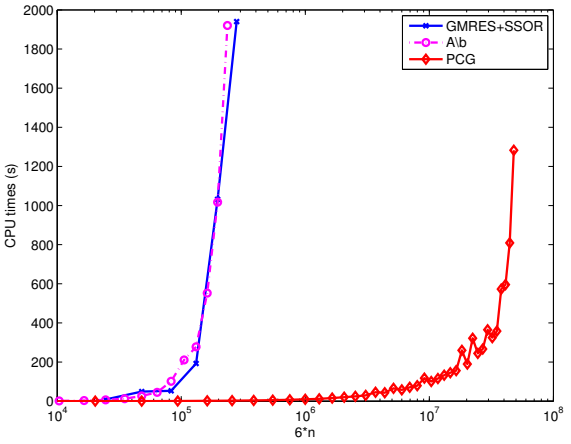

FIG. 5.4. *The time for solving* (5.1) *by left matrix divide and the* `gmres` *and solving* (4.12) *by* `pcg`.

k	$(\frac{1}{4},0,0)$	$(\frac{1}{2},\frac{1}{2},0)$	$(\frac{1}{2},\frac{1}{2},\frac{1}{2})$	$(\frac{1}{4},\frac{1}{4},\frac{1}{4})$
S.I. Arnoldi+LU	18,821	10,533	16,628	20,758
Algorithm 1	155	140	198	155

TABLE 5.1

CPU time in seconds for solving the GEP (3.1). *S.I. Arnoldi+LU stands for the shift-and-invert Arnoldi method with LU based linear system solver. We take* $n_1 = n_2 = n_3 = 32$ *and* $(\varepsilon_i, \varepsilon_o, \gamma) = (13, 1, 0.5)$.

5.2. Comparison with the shift-and-invert Arnoldi method. The GEP (3.1) can be solved using the shift-and-invert Arnoldi method. In the shift-and-invert Arnoldi method, the computational cost is dominated by solving the $6n \times 6n$ linear system

$$\left(\begin{bmatrix} C & 0 \\ 0 & C^* \end{bmatrix} - \sigma \begin{bmatrix} \zeta_d & I_{3n} \\ -\varepsilon_d & -\xi_d \end{bmatrix} \right) y = b, \tag{5.1}$$

for a certain vector b and a shift σ. In contrast, the performance of the null space free method (Algorithm 1) is dominated by solving the $4n \times 4n$ linear system (4.12).

We thus compare the performance for solving these two linear systems. Here, we take $(\varepsilon_i, \varepsilon_o, \gamma) = (13, 1, 1)$ and $\mathbf{k} = [0.5, 0.5, 0]^\top$. To solve (5.1), we use (i) a direct method based on *LU* factorization and (ii) the GMRES with SSOR preconditioner. To solve (4.12), we use the MATLAB `pcg` without preconditioning. Note that the chirality parameter $\gamma = 1$ implies that the coefficient matrix is Hermitian and positive definite. The timing results for solving (5.1) and (4.12) are shown in Figure 5.4. The results suggest that the performance of the `pcg` for solving (4.12) outperforms the two solvers for solving (5.1) remarkably.

In Table 5.1, we further compare the performance of the two eigenvalue solvers: (i) the shift-and-invert Arnoldi method with direct linear system solver and (ii) the null space free method (Algorithm 1) with `pcg`. It is clear that Algorithm 1 is much faster. Consequently, we do not recommend solving the GEP (3.1) by the shift-and-invert Arnoldi method unless we can develop a good preconditioning scheme for solving the linear system (5.1). However, it is important to note that, even with a

good preconditioner, the effect of a large null space (with rank $2n$) can downgrade the performance significantly [12].

5.3. Performance of Algorithm 1. We now concentrate on the performance, in terms of iteration numbers and timing, of the null space free method (Algorithm 1) in finding the 10 smallest positive eigenvalues of the GEP (3.1) with various combinations of the parameters ε_i, γ, and $\mathbf{k}$. We take $n_1 = n_2 = n_3 = 128$, and the size of the coefficient matrix in (4.9) is $4n_1^3 = 8,388,608$. The Lanczos method is applied to solve the HHPD-NFGEP (4.9).

In the first test problem set, we vary the wave vector $2\pi\mathbf{k}$ along the segments connecting G, X, M, R, and G in the first Brillouin zone to plot the band structure. In each of the segments, ten uniformly distributed sampling wave vectors are chosen. The results are shown in Figure 5.5 for $(\varepsilon_i, \varepsilon_o, \gamma) = (13, 1, 0.5)$ or $(\varepsilon_i, \varepsilon_o, \gamma) = (1, 1, 0.8)$. In the second test problem set, we change the chirality parameter γ from 0.25 to 3 for $\varepsilon_i = 13$ (from $\gamma = 0.05$ to 0.9 for $\varepsilon_i = 1$). Note that the condition number of the linear system (4.12) increases from $\frac{\varepsilon_i}{\varepsilon_o} = 13$ to ∞ (singular) as γ varies from 0 to $\sqrt{\varepsilon_i} \approx 3.61$. We fix $\mathbf{k} = [0.5, 0, 0]^\top$. The results are shown in Figure 5.6. Based on Figures 5.5 and 5.6, we highlight the following performance results.

- **The iteration numbers are very small.** Figures 5.5(c), 5.5(d) 5.6(c), and 5.6(d) show the iteration numbers of the Lanczos method for solving (4.9) with different parameter combinations. In all cases, the iteration numbers are substantially smaller than the matrix size $8,388,608$. Note that some higher iteration numbers in Figures 5.5(c) and 5.5(d) are due to the corresponding multiplicity of eigenvalues. The higher iteration numbers in Figures 5.6(c) and 5.6(d) are due to the clustering of the eigenvalues.
- **The timing is satisfactory.** Figures 5.5(e) and 5.5(f) show the CPU times for solving (3.1). These results suggest that our approach is efficient for computing 10 (interior) eigenvalue problems as large as $8,388,608$. This efficiency is mainly due to the highly efficient linear system solver for (4.12).
- **The linear systems in the form of** (4.12) **are well-conditioned for the tested γ's.** We take a close look of the behavior of `pcg` for solving the linear systems (4.12) with various γ's. As shown in Figures 5.6(g) and 5.6(h), the (average) `pcg` iteration numbers for solving linear system (4.12) in the tested eigenvalue problems increase from 39 to 90 for $\varepsilon_i = 13$ and increase from 9 to 59 for $\varepsilon_i = 1$. This behavior is parallel to the increase in the condition number of the linear system (4.12) from $\frac{\varepsilon_i}{\varepsilon_o} = 13$ to ∞ (singular) as γ varies from 0 to $\sqrt{\varepsilon_i} \approx 3.61$. We fix $\mathbf{k} = [0.5, 0, 0]^\top$. A more important observation is that the timing results are quite satisfactory in the following sense. For problems as large as 8.4 million and a stopping tolerance as small as 10^{-14}, these small iteration numbers suggest that the coefficient matrix in (4.12) is quite well-conditioned.

6. Conclusions. In this paper, we focus on the generalized eigenvalue problems (GEP) arising in the source-free Maxwell equation with magnetoelectric coupling effects in the 3D chiral media. Solving the GEP is a computational challenge. We have proposed a promising theoretical framework for efficiently solving the eigenvalue problem. First, we derive the singular value decomposition (SVD) of the discrete single-curl operator. Using this SVD, we explore an explicit form of the basis for the invariant subspace corresponding to nonzero eigenvalues of the GEP. By applying the basis, the GEP is reduced to a null space free standard eigenvalue problem (NFSEP),

which involves only the eigenspace associated with the nonzero eigenvalues of the GEP and excludes the zero eigenvalues so that they do not degrade the computational efficiency. Next, we show that all nonzero eigenvalues of the GEP are real if μ_d and $\varepsilon_d - \xi_d \mu_d^{-1} \zeta_d$ are Hermitian positive definite and $\xi_d^* = \zeta_d$. Based on this property, we reformulate the NFSEP to a null space free generalized eigenvalue problem whose coefficient matrices are Hermitian and Hermitian positive definite (HHPD-NFGEP). We can then use the invert Lanczos method to solve the HHPD-NFGEP and the conjugate gradient (CG) method to solve the embedded linear systems. The numerical results validate the correctness of the proposed algorithms and the computer code implementation. The results also suggest that the proposed methods are efficient in terms of iteration and timing.

Appendix. Proof of Lemma 2.2:
(a). For the sake of contradiction, it is assumed that Λ_q is singular. By the definition of Λ_q, Λ_q is singular if and only if $\Lambda_{\mathbf{a}_1,n_1}$, $\Lambda_{\mathbf{a}_2,n_2}$ and $\Lambda_{\mathbf{a}_3,n_3}$ are singular if and only if

$$\begin{aligned} e^{\theta_{n_1,i}+\theta_{\mathbf{a}_1,n_1}} - 1 &= 0, \\ e^{\theta_{n_2,j}+\theta_{\mathbf{a}_2,n_2}} - 1 &= 0, \\ e^{\theta_{n_3,k}+\theta_{\mathbf{a}_3,n_3}} - 1 &= 0 \end{aligned}$$

for some $i \in \{0,\ldots,n_1-1\}$, $j \in \{0,\ldots,n_2-1\}$ and $k \in \{0,\ldots,n_3-1\}$. That is

$$\frac{i+\mathbf{k}\cdot\mathbf{a}_1}{n_1} = \frac{i+\mathrm{k}_1}{n_1}, \quad \frac{j+\mathbf{k}\cdot\mathbf{a}_2}{n_2} = \frac{j+\mathrm{k}_2}{n_2}, \frac{k+\mathbf{k}\cdot\mathbf{a}_3}{n_3} = \frac{k+\mathrm{k}_3}{n_3}$$

are integers for some i,j,k. By the assumption $0 \le \mathrm{k}_1, \mathrm{k}_2, \mathrm{k}_3 \le \frac{1}{2}$, we have $i=0$, $j=0$, $k=0$ and $\mathrm{k}_1 = \mathrm{k}_2 = \mathrm{k}_3 = 0$ which contradict to $\mathbf{k} \neq 0$. Therefore, Λ_q is nonsingular.

(b). By the definitions of Λ_1, Λ_2 and Λ_3 in (2.10), the $((k-1)n_1n_2+(j-1)n_1+i)$th elements of Λ_1, Λ_2 and Λ_3 are

$$\delta_x^{-1}(e^{\theta_i}-1), \quad \delta_y^{-1}(e^{\theta_j}-1), \quad \delta_z^{-1}(e^{\theta_k}-1),$$

respectively, where

$$\theta_i = 2\pi\left(\frac{i+\mathrm{k}_1}{n_1}\right), \quad \theta_j = 2\pi\left(\frac{j+\mathrm{k}_2}{n_2}\right), \quad \theta_k = 2\pi\left(\frac{k+\mathrm{k}_3}{n_3}\right),$$

for $i=0,\ldots,n_1-1$, $j=0,\ldots,n_2-1$ and $k=0,\ldots,n_3-1$. Assume that Λ_p does not have full column rank. Then there exists some i, j and k such that

$$\begin{aligned} \beta\delta_z^{-1}(e^{\mathrm{i}\theta_k}-1) &= \delta_y^{-1}(e^{\mathrm{i}\theta_j}-1), \\ \delta_x^{-1}(e^{\mathrm{i}\theta_i}-1) &= \alpha\delta_z^{-1}(e^{\mathrm{i}\theta_k}-1), \\ \beta\delta_x^{-1}(e^{\mathrm{i}\theta_i}-1) &= \alpha\delta_y^{-1}(e^{\mathrm{i}\theta_j}-1), \end{aligned}$$

which implies that

$$\frac{\beta\sin\theta_k}{\delta_z} = \frac{\sin\theta_j}{\delta_y}, \quad \frac{\sin\theta_i}{\delta_x} = \frac{\alpha\sin\theta_k}{\delta_z}, \quad \frac{\beta\sin\theta_i}{\delta_x} = \frac{\alpha\sin\theta_j}{\delta_y}$$

and

$$\frac{\beta(\cos\theta_k-1)}{\delta_z}=\frac{\cos\theta_j-1}{\delta_y},$$
$$\frac{\cos\theta_i-1}{\delta_x}=\frac{\alpha(\cos\theta_k-1)}{\delta_z},$$
$$\frac{\beta(\cos\theta_i-1)}{\delta_x}=\frac{\alpha(\cos\theta_j-1)}{\delta_y}$$

or equivalent to

$$\frac{\beta\sin\theta_i}{\alpha\delta_x}=\frac{\sin\theta_j}{\delta_y}=\frac{\beta\sin\theta_k}{\delta_z} \tag{6.1}$$

and

$$\frac{\beta(\cos\theta_i-1)}{\alpha\delta_x}=\frac{\cos\theta_j-1}{\delta_y}=\frac{\beta(\cos\theta_k-1)}{\delta_z}. \tag{6.2}$$

From (6.1) and (6.2), it holds that

$$\left(\frac{\beta\sin\theta_i}{\alpha\delta_x}\right)^2+\left(\frac{\beta(\cos\theta_i-1)}{\alpha\delta_x}\right)^2=\left(\frac{\sin\theta_j}{\delta_y}\right)^2+\left(\frac{\cos\theta_j-1}{\delta_y}\right)^2$$
$$=\left(\frac{\beta\sin\theta_k}{\delta_z}\right)^2+\left(\frac{\beta(\cos\theta_k-1)}{\delta_z}\right)^2$$

and then

$$\frac{\beta^2(2-2\cos\theta_i)}{\alpha^2\delta_x^2}=\frac{2-2\cos\theta_j}{\delta_y^2}=\frac{\beta^2(2-2\cos\theta_k)}{\delta_z^2}.$$

Therefore,

$$\frac{\beta(\cos\theta_i-1)}{\alpha\delta_x}=\frac{\alpha\delta_x}{\beta\delta_y}\frac{\cos\theta_j-1}{\delta_y},\quad \frac{\beta(\cos\theta_k-1)}{\delta_z}=\frac{\delta_z}{\beta\delta_y}\frac{\cos\theta_j-1}{\delta_y}. \tag{6.3}$$

From (6.2) and (6.3), we can see that if $\alpha\delta_x\neq\beta\delta_y$ and $\delta_z\neq\beta\delta_y$, then

$$\cos\theta_i=\cos\theta_j=\cos\theta_k=1.$$

That is $\frac{i+\mathrm{k}_1}{n_1}$, $\frac{j+\mathrm{k}_2}{n_2}$ and $\frac{k+\mathrm{k}_3}{n_3}$ must be integers. This contradicts to the assumption for $\mathbf{k}$. Therefore, Λ_p has full column rank.

Acknowledgements. The authors appreciate the anonymous referees for their useful comments and suggestion. This work is partially supported by the National Science Council, the National Center for Theoretical Sciences, the Taida Institute for Mathematical Sciences, and the Chiao-Da ST Yau Center in Taiwan.

REFERENCES

[1] X. Cheng, H. Chen, L. Ran, B.-I. Wu, T. M Grzegorczyk, and J. A. Kong. Negative refraction and cross polarization effects in metamaterial realized with bianisotropic s-ring resonator. Phys. Rev. B, 76(2):024402, 2007.

[2] R.-L. Chern. Anomalous dispersion in pseudochiral media: Negative refraction and backward wave. J. Phys. D: Appl. Phys., 46:125307, 2013.
[3] R.-L. Chern. Wave propagation in chiral media: composite Fresnel equations. J. Opt., 15:075702, 2013.
[4] R.-L. Chern and P.-H. Chang. Negative refraction and backward wave in chiral mediums: Illustrations of Gaussian beams. J. Appl. Phys., 113:153504, 2013.
[5] R.-L. Chern and P.-H. Chang. Negative refraction and backward wave in pseudochiral mediums: illustrations of Gaussian beams. Opt. Express, 21:2657–2666, 2013.
[6] R.-L. Chern and P.-H. Chang. Wave propagation in pseudochiral media: Generalized Fresnel equations. J. Opt. Soc. Amer. B, 30:552–558, 2013.
[7] R.L. Chern, C.Chung Chang, Chien-C. Chang, and R.R. Hwang. Numerical study of three-dimensional photonic crystals with large band gaps. J. Phys. Soc. Japan, 73:727–737, 2004.
[8] J. Chongjun, Q. Bai, Y. Miao, and Q. Ruhu. Two-dimensional photonic band structure in the chiral medium-transfer matrix method. Opt. Commun., 142:179–183, 1997.
[9] C. Engström and M. Richter. On the spectrum of an operator pencil with applications to wave propagation in periodic and frequency dependent materials. SIAM J. Appl. Math., 70(1):231–247, 2009.
[10] P.-F. Hsieh, T.-T. Wu, and J.-H. Sun. Three-dimensional phononic band gap calculations using the FDTD method and a pc cluster system. IEEE Trans. Ultrason. Ferroelectr. Freq. Control, 53:148–158, 2006.
[11] T.-M. Huang, H.-E. Hsieh, W.-W. Lin, and W. Wang. Eigendecomposition of the discrete double-curl operator with application to fast eigensolver for three dimensional photonic crystals. SIAM J. Matrix Anal. Appl., 34:369–391, 2013.
[12] T.-M. Huang, H.-E. Hsieh, W.-W. Lin, and W. Wang. Fast lanczos eigenvalue solvers for band structures of three dimensional photonic crystals with face-centered cubic lattice. Technical report, NCTS Preprints in Mathematics, National Tsing Hua University, Hsinchu, Taiwan, 2013-3-003, 2013.
[13] T.-M. Huang, Y.-C. Kuo, and W. Wang. Computing extremal eigenvalues for three-dimensional photonic crystals with wave vectors near the Brillouin zone center. J. Sci. Comput., 55:529–551, 2013.
[14] T.-M. Huang, W.-W. Lin, and W. Wang. Matrix representation of discrete differential operators and operations in electromagnetism. Technical report, NCTS Preprints in Mathematics, National Tsing Hua University, Hsinchu, Taiwan, 2014-8-003, 2014.
[15] J. D. Joannopoulos, S. G. Johnson, J. N. Winn, and R. D. Meade. Photonic Crystals: Molding the Flow of Light. Princeton University Press, Princeton, NJ, 2008.
[16] E. O. Kamenetskii. Theory of bianisotropic crystal lattices. Phys. Rev. E, 57:3563–3573, 1998.
[17] C. Kittel. Introduction to solid state physics. Wiley, New York, 2005.
[18] Jin Au Kong. Theorems of bianisotropic media. Proc. IEEE, 60(9):1036–1046, 1972.
[19] J. Lekner. Optical properties of isotropic chiral media. Pure Appl. Opt., 5:417–443, 1996.
[20] S.-Y. Lin, J. G. Fleming, R. Lin, M. M. Sigalas, R. Biswas, and K. M. Ho. Complete three-dimensional photonic bandgap in a simple cubic structure. J. Opt. Soc. Amer. B, 18:32–35, 2001.
[21] Y. Liu and X. Zhang. Metamaterials: a new frontier of science and technology. Chem. Soc. Rev., 40:2494–2507, 2011.
[22] T. G Mackay and A. Lakhtakia. Negative refraction, negative phase velocity, and counterposition in bianisotropic materials and metamaterials. Phys. Rev. B, 79(23):235121, 2009.
[23] M. Reed and B. Simon. Methods of modern mathematical physics. In Analysis of Operators IV. Academic Press, San Diego, CA, 1978.
[24] K. Schmidt and R. Kappeler. Efficient computation of photonic crystal waveguide modes with dispersive material. Opt. Express, 18(7):7307–7322, 2010.
[25] K. Schmidt and P. Kauf. Computation of the band structure of two-dimensional photonic crystals with hp finite elements. Comput. Methods Appl. Mech. Engrg., 198(13):1249–1259, 2009.
[26] A. Serdyukov, I. Semchenko, S. Tretyakov, and A. Sihvola. Electromagnetics of Bi-anisotropic Materials: Theory and Applications. Gordon and Breach Science, New York, 2001.
[27] A. H. Sihvola, A. J. Viitanen, I. V. Lindell, and S. A. Tretyakov. Electromagnetic Waves in Chiral and Bi-Isotropic Media. Artech House, Boston, 1994.
[28] S. A. Tretyakov, A. H. Sihvola, A. A. Sochava, and C. R. Simovski. Magnetoelectric interactions in bi-anisotropic media. J. Electromagn. Waves Appl., 12:481–497, 1998.
[29] S. A Tretyakov, C. R. Simovski, and M. Hudlička. Bianisotropic route to the realization and matching of backward-wave metamaterial slabs. Phys. Rev. B, 75(15):153104, 2007.

[30] B. Wang, J. Zhou, T. Koschny, M. Kafesaki, and C. M Soukoulis. Chiral metamaterials: simulations and experiments. J. Opt. A: Pure Appl. Opt., 11:114003, 2009.

[31] W. S. Weiglhofer and A. Lakhtakia. Introduction to Complex Mediums for Optics and Electromagnetics. SPIE, Washington, DC, 2003.

[32] K. Yee. Numerical solution of initial boundary value problems involving Maxwell's equations in isotropic media. IEEE Trans. Antennas and Propagation, 14:302–307, 1966.

[33] R. Zhao, T. Koschny, and C.M. Soukoulis. Chiral metamaterials: retrieval of the effective parameters with and without substrate. Optics Express, 18:14553–14567, 2010.

[34] N. Zhou, J. V. Clark, and K. S. J. Pister. Nodal simulation for MEMS design using SUGAR v0.5. In Proceedings of International Conference on Modeling and Simulation of Microsystems Semiconductors, Sensors and Actuators, Santa Clara, CA, pp. 308-313, 1998.

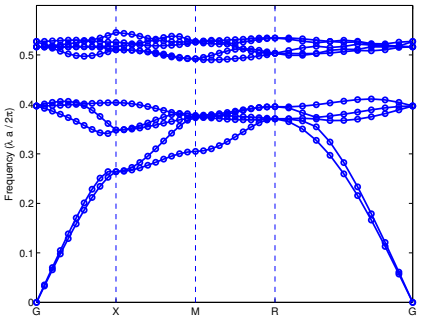

(a) Band structure for $(\varepsilon_i, \varepsilon_o, \gamma) = (13, 1, 0.5)$

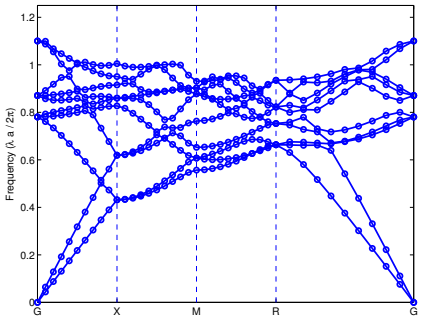

(b) Band structure for $(\varepsilon_i, \varepsilon_o, \gamma) = (1, 1, 0.8)$

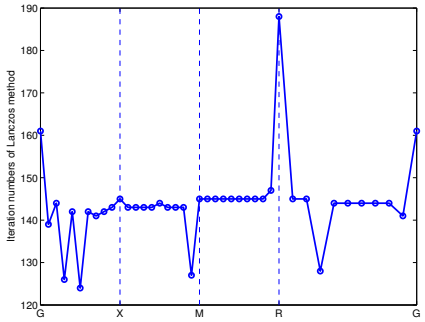

(c) Iteration numbers ranging from 120 to 190 with average 143 for $(\varepsilon_i, \varepsilon_o, \gamma) = (13, 1, 0.5)$

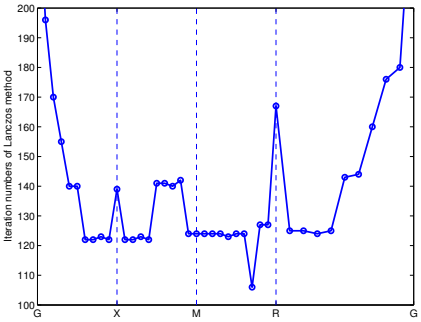

(d) Iteration numbers ranging from 100 to 200 with average 136 for $(\varepsilon_i, \varepsilon_o, \gamma) = (1, 1, 0.8)$

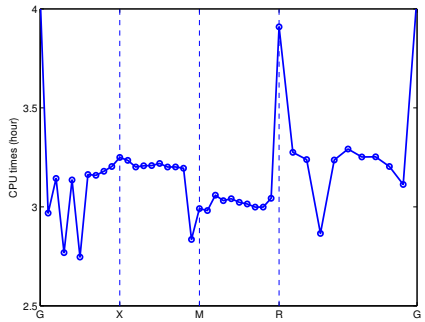

(e) CPU time ranging from 2.75 to 4 hours with average 3.2 hours for $(\varepsilon_i, \varepsilon_o, \gamma) = (13, 1, 0.5)$

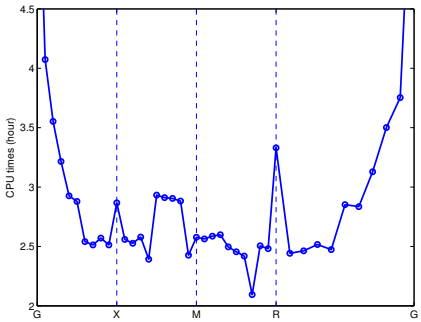

(f) CPU time ranging from 2.1 to 4.1 hours with average 2.8 hours for $(\varepsilon_i, \varepsilon_o, \gamma) = (1, 1, 0.8)$

FIG. 5.5. *The band structures of 3D chiral media, iteration number of the Lanczos method and the elapsed times of the NSF (Algorithm 1) for solving* (3.1) *associated with various wave vectors* $\mathbf{k}$.

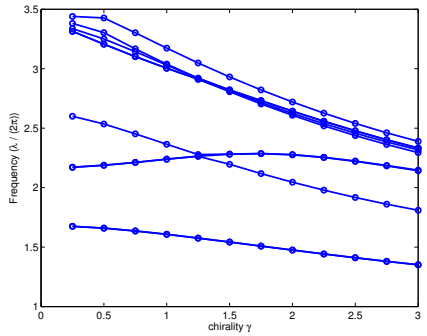

(a) Band structure for $(\varepsilon_i, \varepsilon_o, \gamma) = (13, 1, \gamma)$

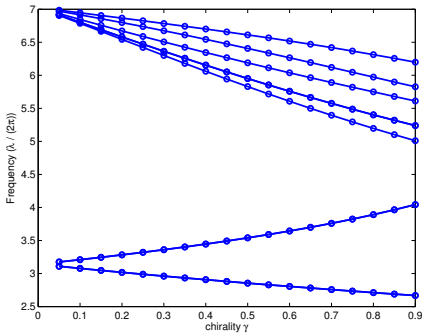

(b) Band structure for $(\varepsilon_i, \varepsilon_o, \gamma) = (1, 1, \gamma)$

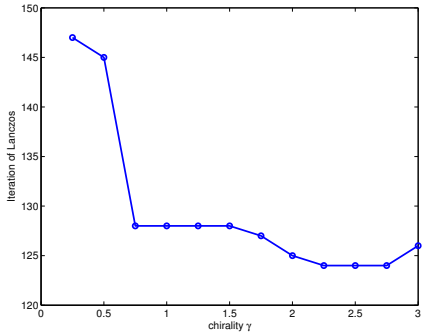

(c) Iteration numbers ranging from 124 to 147 for $(\varepsilon_i, \varepsilon_o, \gamma) = (13, 1, \gamma)$

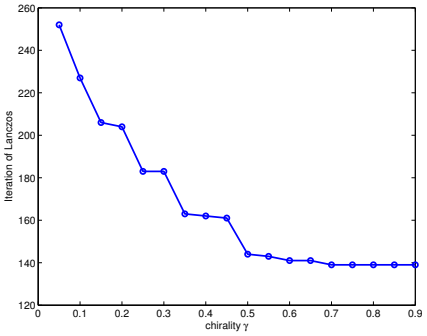

(d) Iteration numbers ranging from 140 to 260 for $(\varepsilon_i, \varepsilon_o, \gamma) = (1, 1, \gamma)$

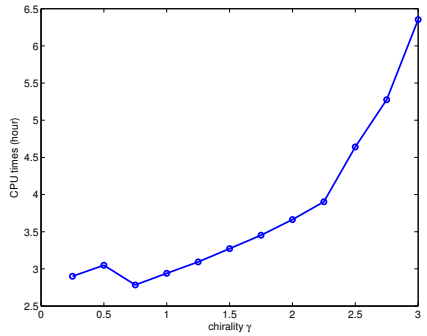

(e) CPU time increasing from 2.5 to 6.5 hours for $(\varepsilon_i, \varepsilon_o, \gamma) = (13, 1, \gamma)$

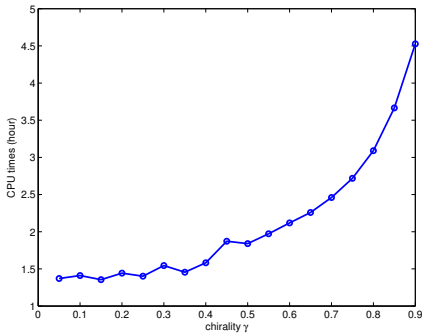

(f) CPU time increasing from 1.4 to 4.5 hours for $(\varepsilon_i, \varepsilon_o, \gamma) = (1, 1, \gamma)$

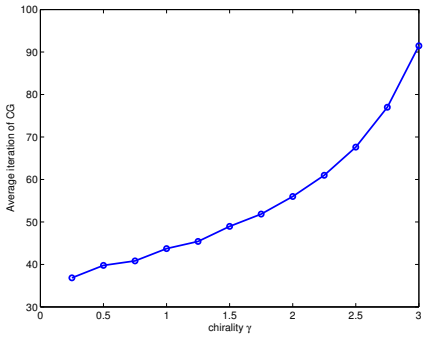

(g) Iteration numbers of CG for $(\varepsilon_i, \varepsilon_o, \gamma) = (13, 1, \gamma)$

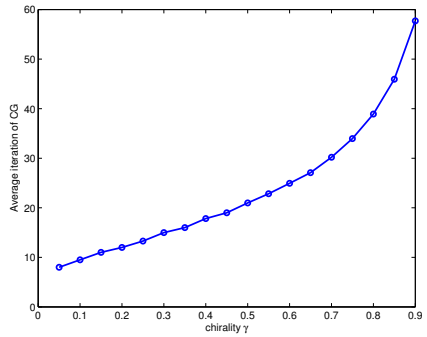

(h) Iteration numbers of CG for $(\varepsilon_i, \varepsilon_o, \gamma) = (1, 1, \gamma)$

FIG. 5.6. *The band structures of 3D chiral media, the average of iteration number of* `pcg`*, the iteration numbers of the Lanczos method and the elapsed times of the NSF for solving* (3.1) *associated with various chirality parameters* γ.